Molecules and Cells

Loss of Primary Cilia Results in the Development of Cancer in the Murine Thyroid Gland

Junguee Lee[1], Shinae Yi[2], Joon Young Chang[2], Jung Tae Kim[2], Hae Joung Sul[1], Ki Cheol Park[3], Xuguang Zhu[4], Sheue-yann Cheng[4], Jukka Kero[5], Joon Kim[6], and Minho Shong[2,*]

[1]Department of Pathology, Daejeon St. Mary's Hospital, College of Medicine, The Catholic University of Korea, Daejeon 34943, Korea, [2]Research Center for Endocrine and Metabolic Diseases, Division of Endocrinology, Department of Internal Medicine, Chungnam National University School of Medicine, Daejeon 35015, Korea, [3]Clinical Research Institute, Daejeon St. Mary's Hospital, College of Medicine, The Catholic University of Korea, Daejeon 34943, Korea, [4]Laboratory of Molecular Biology, National Cancer Institute, MD 20892-4264, USA, [5]Research Centre for Integrative Physiology and Pharmacology, Institute of Biomedicine, University of Turku, 20520 Turku, Finland, [6]Graduate School of Medical Science and Engineering, Korea Advanced Institute of Science and Technology, Daejeon 34040, Korea
*Correspondence: minhos@cnu.ac.kr
http://dx.doi.org/10.14348/molcells.2018.0430
www.molcells.org

Communications at the interface between the apical membrane of follicular cells and the follicular lumen are critical for the homeostasis of thyroid gland. Primary cilia at the apical membrane of thyroid follicular cells may sense follicular luminal environment and regulate follicular homeostasis, although their role *in vivo* remains to be determined. Here, mice devoid of primary cilia were generated by thyroid follicular epithelial cell-specific deletion of the gene encoding intraflagellar transport protein 88 (*Ift88*). Thyroid follicular cell-specific *Ift88*-deficient mice showed normal folliculogenesis and hormonogenesis; however, those older than 7 weeks showed irregularly dilated and destroyed follicles in the thyroid gland. With increasing age, follicular cells with malignant properties showing the characteristic nuclear features of human thyroid carcinomas formed papillary and solid proliferative nodules from degenerated thyroid follicles. Furthermore, malignant tumor cells manifested as tumor emboli in thyroid vessels. These findings suggest that loss-of-function of *Ift88*/primary cilia results in malignant transformation from degenerated thyroid follicles.

Keywords: defective ciliogenesis, dilated and destroyed thyroid follicle, malignant transformation, primary cilia

INTRODUCTION

The mammalian thyroid gland is composed of globular shaped, vascular encircled, and colloid filled follicles that are indispensable for the functional integrity of the thyroid gland. The apical, colloid facing membrane of follicular epithelial cells is an active exchange interface involved in hormonogenesis. Primary cilia are a specialized sensory organelle that projects from the apical membrane of polarized follicular epithelial cells into the follicular lumen (Christensen et al., 2007; Lee et al., 2016). Primary cilia in thyroid follicles may sense the follicular luminal environment and transmit signals to epithelial cells to maintain follicular homeostasis. The thyroid phenotypes of ciliopathy, a genetic disorder affecting ciliary function, are characterized by a broad range of thyroid dysfunction, suggesting that primary cilia perform pivotal roles in the thyroid gland (Ferkol and Leigh, 2012). However, the thyroid-specific function of primary cilia *in vivo* remains to be determined. Therefore, it is important to elucidate the exact role of primary cilia in the functional homeostasis and structural integrity of thyroid follicles.

Studies of the distribution and expression pattern of primary cilia show that cancer cells have reduced or absent

Received 21 November, 2018; revised 25 November, 2018; accepted 26 November, 2018; published online 2 January, 2019

eISSN: 0219-1032
© The Korean Society for Molecular and Cellular Biology. All rights reserved.
This is an open-access article distributed under the terms of the Creative Commons Attribution-NonCommercial-ShareAlike 3.0 Unported License. To view a copy of this license, visit http://creativecommons.org/licenses/by-nc-sa/3.0/.

primary cilia (Egeberg et al., 2012; Han et al., 2009; Hassounah et al., 2013; Kim et al., 2011; Menzl et al., 2014; Schraml et al., 2009; Seeley et al., 2009; Wong et al., 2009). Furthermore, dysfunction of the primary cilium and defects in ciliogenesis are associated with tumor progression (Bailey et al., 2009; Hassounah et al., 2012; Kobayashi et al., 2017; Radford et al., 2012). The progression of tumors associated with ciliogenesis defects is linked to the constitutive activation of the Wnt/β-catenin pathway (Han and Alvarez-Buylla, 2010; Han et al., 2009; Radford et al., 2012). Although ciliogenesis defects are frequently detected in cancer cells, the direct functional consequence of ciliary dysfunction on tumor development remains to be established *in vivo*.

To investigate the effect of primary cilia on the structural integrity of thyroid follicles, we generated mice in which ciliogenesis was specifically inactivated in thyroid follicular cells. Loss of primary cilia was induced by inactivation of the intraflagellar transport protein 88 (*Ift88*) gene using a thyroglobulin (Tg) promoter-driven *Cre*-recombinase. Intraflagellar transport 88 (IFT88) is a subunit of the IFT-B complex that plays an essential role in anterograde transport of ciliary proteins. We previously showed that loss-of-function (LOF) of IFT88 uniformly result in ciliary loss in thyroid cancer cell lines (Lee et al., 2018). IFT88 is also known to function as a tumor suppressor in hepatocellular carcinoma, breast carcinoma, and basal cell carcinoma (Bonura et al., 1999; Wong et al., 2009). Thyroid of transgenic mice (*Tg-Cre;Ift88*$^{flox/flox}$ mice) showed a marked defect in ciliogenesis and were characterized by irregularly dilated and destroyed follicles. Furthermore, these mice developed papillary-solid proliferative thyroid follicles with malignant features. These results indicate that primary cilia in the murine thyroid gland play a critical role in maintaining follicular structural integrity, and loss-of-function (LOF) of primary cilia contributes to malignant transformation.

MATERIALS AND METHODS

Human normal and malignant thyroid follicular cell lines

The human thyroid cell lines Nthy-ori 3-1 (ECACC) and the anaplastic thyroid cancer cell line 8505C (BRAF^{V600E}-mutant) were cultured in RPMI1640 (Gibco®) medium containing 10% fetal bovine serum (FBS) and 1% penicillin-streptomycin (PS). The papillary thyroid cancer cell lines TPC1 (RET/PTC1 rearrangements) and BCPAP (BRAF^{V600E}-mutant), and the anaplastic thyroid cancer cell lines SW1736 (BRAF^{V600E}-mutant) and HTh7 (NRAS^{Q61R}-mutant), were cultured in DMEM (Gibco®) with 10% FBS and 1% PS.

Mice

Floxed *Ift88* mice (*Ift88*$^{flox/flox}$, obtained from Dr. Kim J) and thyroglobulin-Cre mice (*Tg-Cre*, *Tg*$^{Cre/+}$, obtained from Dr. Jukka Kero) were of the C57BL/6 genetic background. *Ift88*$^{flox/flox}$ mice were crossed with *Tg-Cre* transgenic mice to generate thyroid gland-specific *Ift88*-knockout (*Tg-Cre;Ift88*$^{flox/flox}$) mice. Only male mice were used in the current study. All animal experiments received prior approval by the Institutional Animal Care and Use Committee of the Catholic Medical Center (approval ID, CRCC-BE-CMC-17013391).

Serum hormone assays

Retro-orbitally collected, clotted mouse blood was centrifuged at 3000 g for 10 min. Sera were separated and stored at -20℃ prior to the hormone assay. Free T3 and T4 levels were measured using an ELISA kit (Merck Millipore) according to the manufacturer's instructions. Serum TSH was measured using a specific mouse TSH RIA provided by Dr. Cheng SY (Center for Cancer Research, National Cancer Institute, USA).

Histological analysis

Thyroid tissues were removed from mice, fixed with 10% neutral buffered formalin for 24 h at room temperature, processed, and embedded in paraffin. Paraffin blocks were cut into 4 μm-thick slices. Tissue slices were routinely deparaffinized and stained with hematoxylin and eosin (H&E).

Immunofluorescence

FFPE tissue blocks were cut to 7 μm thickness, and tissue sections were deparaffinized in xylene and rehydrated through a graded series of ethanol baths. The tissue sections were heated in citrate buffer (0.01 M citric acid-sodium citrate, pH 6.0) at 121℃ for 25 min for antigen retrieval. After washing, sections were air-dried for 30 min and then re-washed with 1× phosphate-buffered saline (PBS, 10 mM Na_2HPO_4, pH 7.4, and 150 mM NaCl). The tissue sections were fixed with 4% paraformaldehyde in PBS for 15 min, permeabilized with 0.5% Triton X-100 in PBS for 10 min, and then blocked with 5% bovine serum albumin in PBS for 30 min at room temperature. Thereafter, tissue sections were incubated with primary antibodies for 12 h at 4℃. Lists of primary antibodies are as follows; ARL13B (ProteinTech Group), GT335 (AdipoGen), γ-tubulin (Sigma-Aldrich), Cytokeratin (Dako). The tissue-section slides were then washed three times with 1× PBS and incubated with secondary antibodies at 4℃ for 8 h. Goat anti-mouse and goat anti-rabbit secondary antibodies conjugated to Alexa Fluor dyes (Invitrogen/Life Technologies) were used for indirect fluorescent detection. Nuclei were stained with DAPI. The stained slides were observed under an Olympus FluoView FV1000 microscope equipped with a charge-coupled device camera (Olympus Corp.).

Immunohistochemistry

FFPE tissue blocks were cut to 4 μm thickness and incubated at 56℃ for 3 h. Tissue-section slides were stained using the Ventana HX automatic system BenchMark (Ventana Medical Systems, France). All procedures, including antigen retrieval and blocking of endogenous peroxidase activity, were performed automatically by the BenchMark system. The tissue sections were incubated with Thyroglobulin (Santa Cruz Biotechnology) primary antibody (for 32 min at 42℃. Immunoperoxidase staining was performed using the LSAB NeuVision system according to the manufacturer's instructions (Ventana), and tissue sections were counterstained with hematoxylin. Slides were analyzed using an OLYMPUS BX51 microscope.

RNA isolation and RT-qPCR

Total RNA was extracted using TRIzol (Invitrogen). Complementary DNA (cDNA) was synthesized from total RNA using M-MLV Reverse Transcriptase and oligo-dT primers (Invitrogen). Reverse transcription quantitative polymerase chain reaction (RT-qPCR) was performed using QuantiTect SYBR Green PCR Master Mix (QIAGEN). Each reaction was performed in triplicate. The PCR primers used are listed in the Supplementary Table 1. Amplification conditions were as follows: 10 min at 95℃ for enzyme activation, and 40 cycles at 95℃ denaturation for 10 s, 60℃ annealing for 30 s, and 72℃ extension for 30 s. The cycle threshold (Ct) values for GAPDH RNA and that of target genes were measured and calculated using computer software (Life Technologies 7500 software, USA).

Statistical analysis

Group comparisons of categorical variables were evaluated using the linear-by-linear association. The means were compared using the independent sample's *t*-test. Values are presented as the mean ± SEM. *P*-values <0.05 were considered statistically significant. Analyses were performed using SPSS Version 22.0 statistical software (SPSS Inc., USA).

RESULTS

Distribution of primary cilia in human normal thyroid follicular cells and thyroid cancer cell lines

The frequency of primary cilia was examined in human normal thyroid follicular (Nthy-ori 3-1), PTC (TPC1 and BCPAP), and ATC (8505C, SW1736, and HTh7) cell lines under serum starvation conditions. The frequency of cells with primary cilia was 32.60 ± 10.20% in Nthy-ori 3-1, 23.13 ± 3.74% in TPC1, 25.13 ± 4.25% in BCPAP, 12.28 ± 5.63% in 8505C, 12.46 ± 2.38% in SW1736, and 12.52 ± 3.23% in HTh7 cells (Fig. 1A). The frequency of primary cilia in PTC cell lines

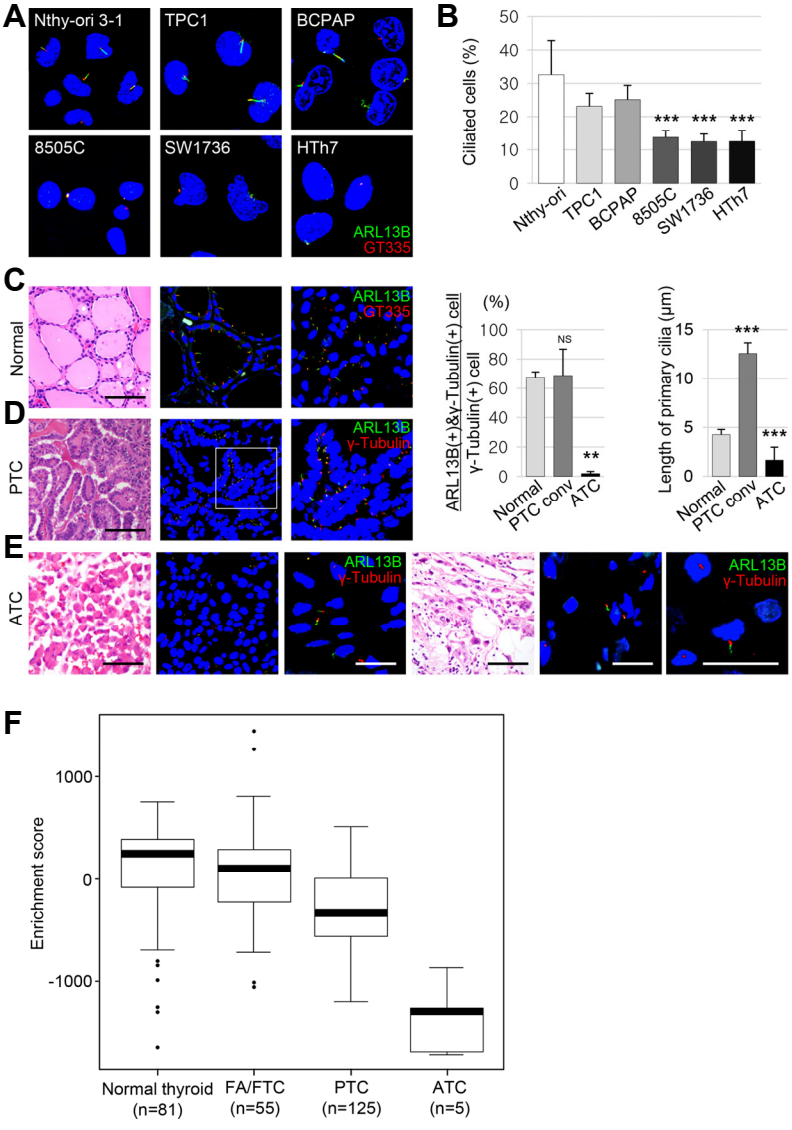

Fig. 1. The expression of primary cilia is decreased in anaplastic thyroid carcinomas (ATCs). (A) Immunofluorescence (IF) analysis of primary cilia using ARL13B (green) for axonemes and GT335 (red) for axonemes with basal bodies. (B) The frequency of primary cilia was 32.60 ± 10.20% in Nthy-ori 3-1, 23.13 ± 3.74% in TPC1, 25.13 ± 4.25% in BCPAP, 12.28 ± 5.63% in 8505C, 12.46 ± 2.38% in SW1736, and 12.52 ± 3.23% in HTh7 cells, respectively. (C, D, E) IF analysis of primary cilia using ARL13B (green) for axonemes and γ-tubulin (red) for basal bodies. The frequency of primary cilia was 67.53 ± 3.62% in normal thyroid follicles, 68.74 ± 18.01% in PTC, and 1.87 ± 1.51% in ATC (normal vs. PTC, $P = 0.2956$; normal vs. ATC, $P < 0.001$). $^{**}P < 0.01$; $^{***}P < 0.001$; NS, not significant. Scale bar: H&E, 100 μm; IF, 5 μm. (F) Activation of primary cilia-specific genes in the normal thyroid and thyroid cancers. Boxplots from the single sample gene set enrichment analysis (ssGSEA) show the activation levels of primary cilia-specific genes in the normal thyroid and in three subtypes of thyroid cancer. Abbreviations: FA/FTC, follicular adenoma/follicular thyroid carcinoma; PTC, papillary thyroid carcinoma; ATC, anaplastic thyroid carcinoma.

(TPC1 and BCPAP) was not statistically significantly different from that in Nthy-ori 3-1 cells (P = 0.0623), whereas the frequency of primary cilia in ATC cell lines was significantly lower than that in Nthy-ori 3-1 (P = 0.0003) or PTC cell lines (P = 0.0008) (Fig. 1B).

Next, the frequency and length of primary cilia were compared between 20 PTC and 20 ATC patients and the normal thyroid. The frequency of primary cilia was significantly lower in ATC (1.87 ± 1.51%) than in normal thyroid follicles (67.53 ± 3.62%) or PTC (68.74 ± 18.01%)(Figs. 1C-1E). The length of primary cilia in normal thyroid follicular cells, PTC, and ATC was 4.26 ± 0.52 μm, 12.57 ± 1.08 μm, and 1.66 ± 1.32 μm, respectively. Primary cilia were longer in conventional PTCs (P < 0.0001) and shorter in ATCs (P < 0.0001) than in the normal thyroid. Taken together, these results indicated that the frequency of primary cilia was comparable between PTC and normal thyroid follicles, whereas the frequency and the length of primary cilia were significantly decreased in ATCs.

In a previous study using the TCGA database (n = 494), we showed that LOF of *IFT88* in PTCs is significantly associated with worse prognostic parameters, such as the tall cell variant, extrathyroidal extension, and lymph node metastasis (Lee et al., 2018). The TNM staging, the MACIS score, and the ATA staging associated with risk of death from thyroid cancer or tumor recurrence were higher in PTCs with low *IFT88* expression (Lee et al., 2018). Here, single sample gene set enrichment analysis (ssGSEA) was performed to determine the activation level of primary cilia-specific genes based

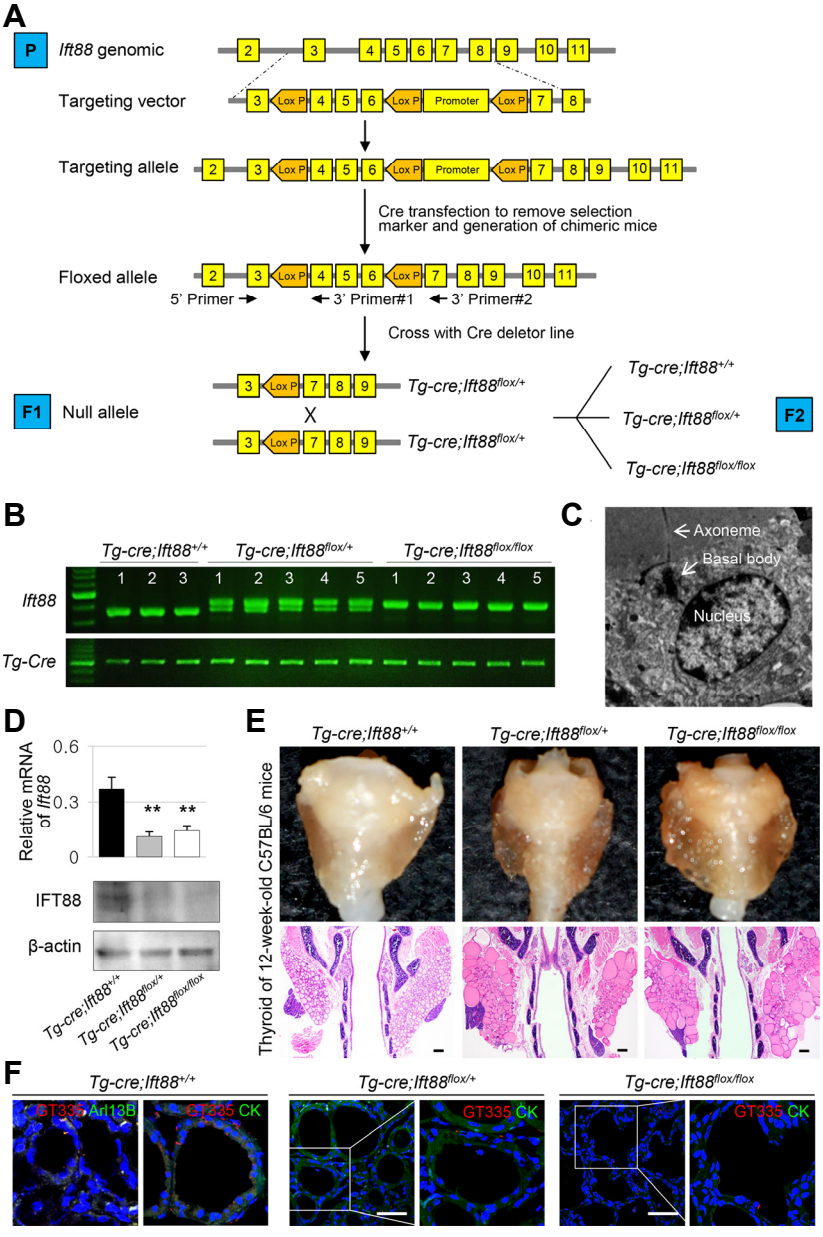

Fig. 2. Thyroid follicular cell-specific *Ift88*-deficient mice exhibit ciliary loss in thyroid follicles. (A) Generation of thyroid follicular cell-specific *Ift88* knockout mice. (B) Analysis of the *Ift88* genotype by PCR from mouse tail DNA. (C) The presence of primary cilia in thyroid follicular cells of *Ift88* wild-type control mice was confirmed by ultrastructural analysis. (D) The expression levels of *Ift88* mRNA and protein were significantly decreased in *Tg-Cre;Ift88*$^{flox/+}$ and *Tg-Cre;Ift88*$^{flox/flox}$ compared with those in the *Tg-Cre;Ift88*$^{+/+}$ thyroid. β-actin was used as the loading control. $**P < 0.01$. (E) Gross morphology and H&E-stained coronal sections of the thyroid in *Ift88*-deficient mice and their wild-type littermates. The thyroid glands from *Ift88*-deficient mice were composed of irregularly shaped follicles of variable size. The control thyroid consisted of homogeneous round follicles. Scale bar: 200 μm. (F) IF analysis of primary cilia using GT335 (red) for axoneme with basal body, Arl13B (green) for axoneme. In the *Tg-Cre;Ift88*$^{+/+}$ thyroid, primary cilia are present in follicular cells. In *Tg-Cre;Ift88*$^{flox/flox}$ and *Tg-Cre;Ift88*$^{flox/+}$ thyroid follicles, primary cilia are almost absent. Scale bar: 10 μm.

on a previous study in PTC, follicular adenoma (FA)/FTC, and ATC compared with the normal thyroid (Fig. 1F)(Yoo et al., 2016). The activation levels of genes involved in ciliogenesis, ciliary assembly, and substrate transport were lower in differentiated thyroid cancer (DTC, such as PTC and FTC) than in the normal thyroid. In particular, the expression of primary cilia-specific genes was significantly lower in ATC cell lines than in normal thyroid and DTC cells.

Taken together, these results indicated that primary cilia were considerably decreased in ATC cell lines and tissues; low IFT88 expression in PTCs was associated with poor prognostic factors, and the expression of primary cilia-specific genes was significantly reduced in ATCs, suggesting that LOF of IFT88/primary cilia affects tumorigenesis or tumor progression in the thyroid.

Thyroid follicular cell-specific *Ift88*-deficient mice show loss of primary cilia in thyroid follicles

IFT88 is a component of IFT particle proteins, which are required for cilium biogenesis and ciliary transport (Katoh et al., 2016; Taschner et al., 2016). To investigate the role of primary cilia in thyroid follicles, we deleted the *Ift88* gene in thyroid follicular cells of mice via *Cre/loxP* recombination (Fig. 2A). In the transgenic mouse strain used for this analysis, the fourth to sixth exons of the *Ift88* gene are flanked by *loxP* sites (*Ift88*$^{flox/flox}$). *Cre*-mediated recombination generates a nonfunctional protein by introducing a frame-shift in the coding region that results in premature termination during translation. To inhibit the formation of primary cilia in thyroid follicular cells, *Ift88*$^{flox/flox}$ mice were crossed with a transgenic mouse line that expresses *Cre*-recombinase under the control of the *Tg* promoter. The endogenous *Tg* gene was expressed in all thyroid follicular cells at mouse embryonic day 14. The expression of *Cre*-recombinase in *Tg-Cre;Ift88*$^{flox/flox}$ transgenic mice was analyzed by PCR (Fig. 2B). The expression of Cre-recombinase and the Ift88 genotypes of the mice were confirmed by PCR analysis of genomic tail DNA (Fig. 2B). Transmission electron microscopy (TEM) confirmed the presence of primary cilium (axoneme with basal body, Fig. 2C). *Tg-Cre;Ift88*$^{flox/flox}$ mice were born and reached adulthood without any sign of compromised health. Reverse transcription quantitative PCR (RT-qPCR) and western blot analyses revealed a significant reduction of *Ift88* mRNA and protein in the mutant thyroid compared with those in the wild-type littermates (Fig. 2D). The control thyroid consisted of homogeneous round follicles, whereas thyroid glands from *Ift88*-deficient mice showed irregularly shaped follicles of variable size (Fig. 2E).

To confirm that *Ift88* inactivation ablates primary cilia formation in thyroid follicular cells, thyroid tissue sections (1-35 week-old mice) were stained with Arl13B for the detection of axoneme and GT335 for the detection of axoneme with basal body. In the *Tg-Cre;Ift88*$^{+/+}$ thyroid, the primary cilium protruded from the apical surface of follicular cells into the

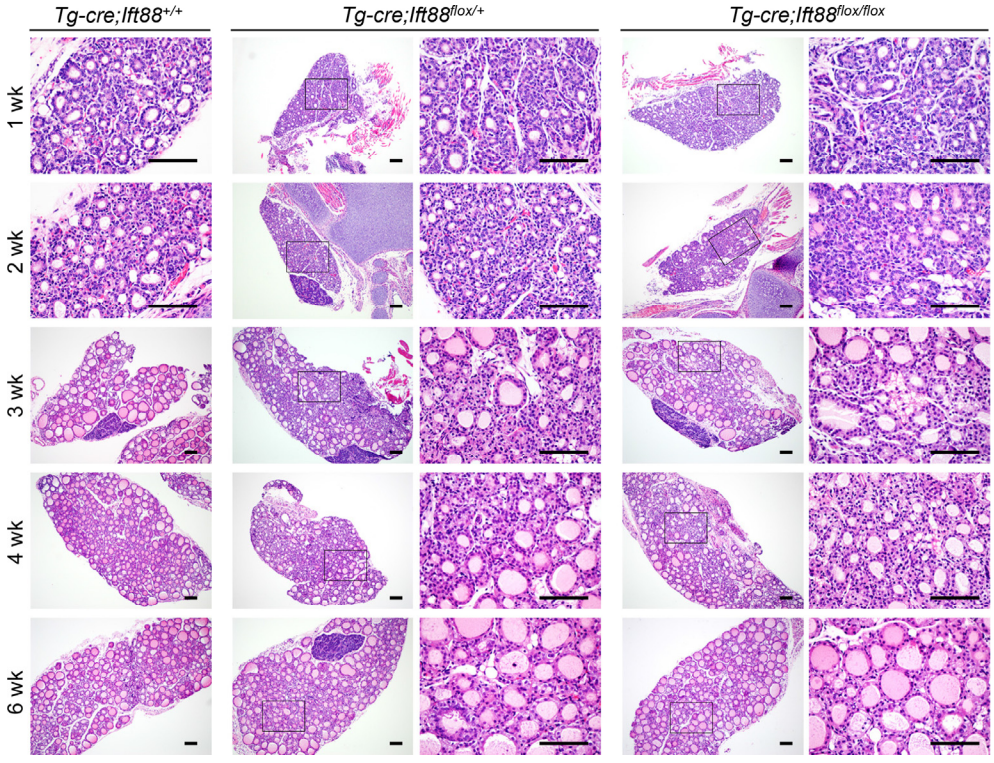

Fig. 3. Deletion of the Ift88 gene in the mouse thyroid is unlikely to be involved in thyroid follicle development. Until 6 weeks of age, the thyroids of homozygous (*Tg-cre;Ift88*$^{flox/flox}$) and heterozygous (*Tg-Cre;Ift88*$^{flox/+}$) mice were phenotypically and functionally indistinguishable from those of the wild-type (*Tg-Cre;Ift88*$^{+/+}$) littermates. Scale bar: 100 μm.

follicular lumen (Fig. 2F). By contrast, primary cilia were almost absent in *Tg-Cre;Ift88*$^{flox/flox}$ and *Tg-Cre;Ift88*$^{flox/+}$ thyroid follicles (Fig. 2F). These findings indicate that deletion of the *Ift88* gene contributes to loss of primary cilia in murine thyroid follicular epithelial cells.

Deletion of the *Ift88* gene in the mouse thyroid is unlikely to be involved in thyroid follicle development

At 6 weeks of age, the thyroid glands of homozygous and heterozygous mice were phenotypically and functionally indistinguishable from those of the wild-type littermates (Fig. 3). At 1-6 weeks of age, the thyroid glands of the control group had uniformly distributed follicles with minimal variation in size and shape. However, homozygotic and heterozygotic mice showed more variation in the size and shape of the thyroid than the control group (Fig. 3). In the three groups, the thyroid gland showed normal follicular structure, featuring a colloid filled lumen surrounded by a single layer of cuboidal follicular cells at 1-6 weeks. These observations suggest that lack of *Ift88* and primary cilia do not affect the postnatal and early development of the murine thyroid gland.

Thyroid function remains normal in *Tg-Cre;Ift88*$^{flox/flox}$ mice

The serum levels of tri-iodothyronine (T3) and TSH were not significantly different between *Tg-Cre;Ift88*$^{flox/flox}$ (T3 = 0.34 ± 0.14 ng/ml; TSH = 35.60 ± 11.27 ng/ml), *Tg-Cre;Ift88*$^{flox/+}$ (T3 = 0.39 ± 0.06 ng/ml; TSH = 52.89 ± 3.53 ng/ml), and *Tg-Cre;Ift88*$^{+/+}$ mice (T3 = 0.45 ± 0.02 ng/ml; TSH = 44.39 ± 7.71 ng/ml) at 7 weeks of age (Fig. 4A). At 11 weeks of age, the serum levels of T3 and TSH in *Tg-Cre;Ift88*$^{flox/flox}$ (T3 = 0.41 ± 0.04 ng/ml; TSH = 42.99 ± 7.76 ng/ml) and *Tg-Cre;Ift88*$^{flox/+}$ mice (T3 = 0.44 ± 0.12 ng/ml; TSH = 60.89 ± 0.71 ng/ml) were not statistically significantly different from those in *Tg-Cre;Ift88*$^{+/+}$ mice (T3 = 0.45 ± 0.04 ng/ml; TSH = 55.05 ± 20.44 ng/ml). At 14 weeks of age, the serum levels of T3 were significantly lower in *Tg-Cre;Ift88*$^{flox/+}$ mice (0.39 ± 0.12 ng/ml) than in *Tg-Cre;Ift88*$^{+/+}$ mice (0.49 ± 0.09 ng/ml), whereas the serum level of T3 did not differ significantly between *Tg-Cre;Ift88*$^{flox/flox}$ mice (0.43 ± 0.04 ng/ml) and *Tg-Cre;Ift88*$^{+/+}$ mice (0.49 ± 0.09 ng/ml). The serum TSH level in *Tg-Cre;Ift88*$^{flox/flox}$ (39.36 ± 0.66 ng/ml, P = 0.1490) and *Tg-Cre;Ift88*$^{flox/+}$ mice (63.88 ± 22.88 ng/ml, P = 0.2013) was not statistically significantly different from that in *Tg-Cre;Ift88*$^{+/+}$ mice (54.04 ± 17.84 ng/ml).

Assessment of the regulation of thyroid-specific genes in *Tg-Cre;Ift88*$^{flox/flox}$ mice showed that the mRNA levels of Na^+/I^- symporter (*Nis*), Pendrin, thyroid peroxidase (*Tpo*), thyrotropin receptor (*Tshr*), and thyroglobulin (*Tg*) were lower in the *Ift88*-deficient than in the *Tg-Cre;Ift88*$^{+/+}$ thyroid at 10 weeks of age (Fig. 4B).

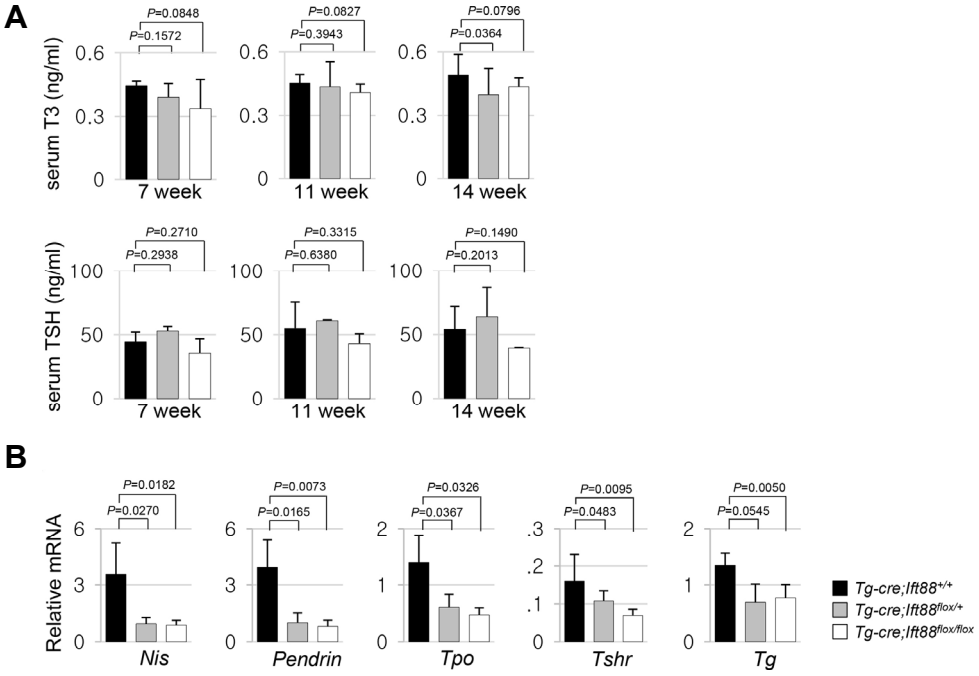

Fig. 4. The expression of thyroid-specific genes is reduced in the thyroid gland of *Tg-Cre;Ift88*$^{flox/flox}$ mice. (A) At 7 weeks of age, the serum levels of T3 and TSH did not differ significantly between *Tg-Cre;Ift88*$^{flox/flox}$, *Tg-Cre;Ift88*$^{flox/+}$, and *Tg-Cre;Ift88*$^{+/+}$ mice. At 11 weeks of age, the serum levels of T3 and TSH in *Tg-Cre;Ift88*$^{flox/flox}$ and *Tg-Cre;Ift88*$^{flox/+}$ mice were not statistically significantly different from those in *Tg-Cre;Ift88*$^{+/+}$ mice. At 14 weeks of age, the serum levels of T3 in *Tg-Cre;Ift88*$^{flox/+}$ mice were significantly lower than those in *Tg-Cre;Ift88*$^{+/+}$ mice, whereas the serum level of T3 in *Tg-Cre;Ift88*$^{flox/flox}$ mice was not significantly different from that in *Tg-Cre;Ift88*$^{+/+}$ mice. Serum TSH in *Tg-Cre;Ift88*$^{flox/flox}$ and *Tg-Cre;Ift88*$^{flox/+}$ mice was not statistically significantly different from that in *Tg-Cre;Ift88*$^{+/+}$ mice. (B) At 10 weeks of age, the mRNA levels of *Nis*, *Pendrin*, *Tpo*, *Tshr*, and *Tg* were lower in the *Tg-Cre;Ift88*$^{flox/+}$ and *Tg-Cre;Ift88*$^{flox/flox}$ thyroid than in the *Tg-Cre;Ift88*$^{+/+}$ thyroid, as measured by RT-qPCR. mRNA was normalized to the expression of *Gapdh*.

Defective *Ift88*-mediated ciliary loss in the murine thyroid causes progressively dilated and destroyed follicles

The gross morphology of the homozygous, heterozygous, and wild-type thyroid glands was unremarkable until week 10. However, histological analysis of H&E-stained *Tg-Cre;Ift88*$^{flox/+}$ thyroid tissue >7 weeks of age showed irregularly dilated follicular lumens lined by a flattened epithelium (Figs. 5A(b)-(d)). The *Tg-Cre;Ift88*$^{flox/flox}$ thyroid also showed irregularly dilated follicles (Figs. 5A(e)-(g)). The thyroid follicular lumens of *Tg-Cre;Ift88*$^{+/+}$ mice were homogeneously filled with colloidal Tg, whereas *Tg-Cre;Ift88*$^{flox/flox}$ mice showed dilated and destroyed follicles with minimal colloid. Intrafollicular Tg staining was nearly negative in these follicles, suggesting decreased Tg production or storage (P = 0.0454, Fig. 5B). The dilated and destroyed follicles in the thyroid of heterozygotes and homozygotes were detected focally until week 11 (Figs. 5C(b)-(d)). At 14 weeks of age, irregularly dilated and destroyed follicles were observed in more than two-thirds of the *Tg-Cre;Ift88*$^{flox/+}$ thyroid (Fig. 5D(c)).

Papillary-solid proliferative follicular cells resembles thyroid carcinoma in *Tg-Cre;Ift88*$^{flox/flox}$ mice

In 11 week-old *Tg-Cre;Ift88*$^{flox/flox}$ mice, the thyroid follicular epithelium exhibited micropapillary hyperplasia (Figs. 5C(c) and (e)-(g)). At 14 weeks of age, the *Tg-Cre;Ift88*$^{flox/flox}$ thyroid was characterized by hyperplastic follicles with papillary infoldings and a small amount of pale colloid (Figs. 5D(d), (f) and (g)). Prominent infoldings of the hyperplastic follicular

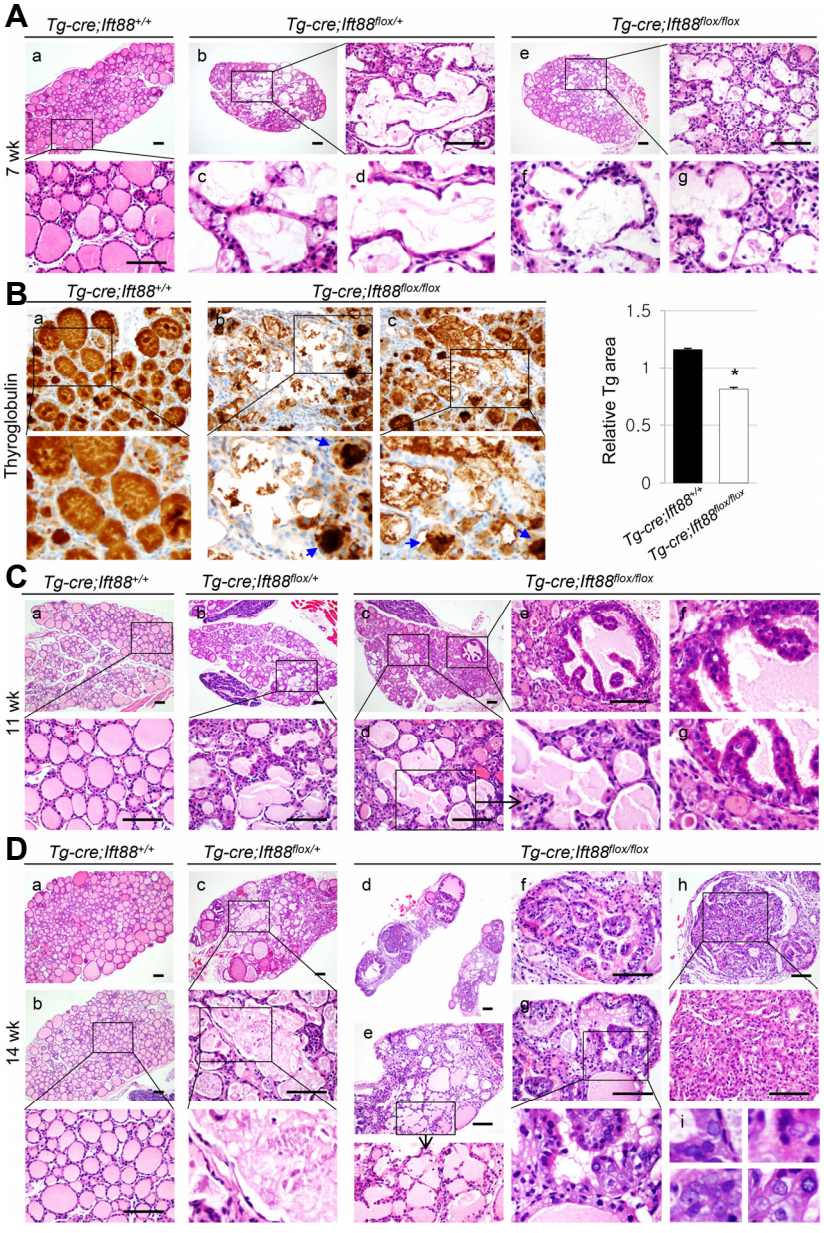

Fig. 5. Loss of function of primary cilia results in the dilated and destroyed follicles in the murine thyroid with defective *Ift88*-mediated ciliary loss. (A) At 7 weeks of age, the *Tg-Cre;Ift88*$^{flox/+}$ (b-d) and *Tg-Cre;Ift88*$^{flox/flox}$ thyroid (e-g) shows irregularly dilated follicles and destroyed follicles. Scale bar: 100 μm. (B) The dilated and destroyed follicles showed colloidal Tg-negative lumens in the *Tg-Cre;Ift88*$^{flox/flox}$ thyroid (a). Small follicular lumens contained compact Tg globules (arrow) in the *Tg-Cre;Ift88*$^{flox/flox}$ thyroid (b, c). $*P < 0.05$. (C) At 11 weeks of age, the dilated and destroyed thyroid follicles in heterozygous and homozygous mice were focally involved. The *Tg-Cre;Ift88*$^{flox/flox}$ thyroid showed micropapillary hyperplasia of the follicular epithelium (b-d). Scale bar: 100 μm. (D) At 14 weeks of age, dilated and destroyed follicles were detected throughout most of the thyroid gland in *Tg-Cre;Ift88*$^{flox/+}$ mice (c). Papillary projections of hyperplastic epithelium were present in the dilated follicles of the *Tg-Cre;Ift88*$^{flox/flox}$ thyroid (d, f-h). Follicular epithelial cells with a papillary growth pattern showed enlarged pleomorphic vesicular nuclei with a groove and prominent nucleoli (i). Scale bar: 100 μm.

epithelium showing disorganization and spindle features were present within the dilated follicles (Fig. 5D(h)). These epithelial cells showing a papillary and solid growth pattern exhibited enlarged pleomorphic vesicular nuclei with a groove and prominent nucleoli, which are consistent with thyroid carcinoma (Fig. 5D(i)). The dilated and destroyed follicles were detected between proliferative follicular nodules in *Tg-Cre;Ift88*$^{flox/flox}$ mice (Figs. 5D(d) and (e)).

The dilated and destroyed follicles rapidly progressed, and by 20 weeks of age, the *Tg-Cre;Ift88*$^{flox/flox}$ thyroid grossly exhibited a bubble wrap-like appearance, manifested histologically as cystically dilated follicles containing colloid (Figs. 6A(a)-(c)). Papillary or solid follicular hyperplasia was associated with scant colloid or clumped Tg globules, which are frequently observed in hypofunctioning thyroid follicles (Figs. 6A(d) and (e)-(h)).

With increasing age, these papillary hyperplastic nodules became larger and eventually occupied nearly the entire thyroid. At 35 weeks of age, the *Tg-Cre;Ift88*$^{flox/flox}$ thyroid exhibited proliferative nodules with a papillary-solid growth pattern (Fig. 6B). The enlarged follicular cells showed nuclear pseudoinclusions (Fig. 6B(g)) and prominent macronucleoli (Fig. 6B(h)). Proliferative follicular nodules infiltrated the perithyroidal skeletal muscle (Figs. 6C(a) and (b)) or parathyroid gland (Fig. 6C(c)). Vascular invasion of tumor emboli was observed in the *Tg-Cre;Ift88*$^{flox/flox}$ thyroid (Fig. 6C(d), arrow). These solid proliferative follicular nodules are considered PDTC. The phenotype of the thyroid in *Tg-Cre;Ift88*$^{flox/flox}$ mice is summarized by age group in Fig. 6D. The incidence of thyroid cancer, as represented by papillary

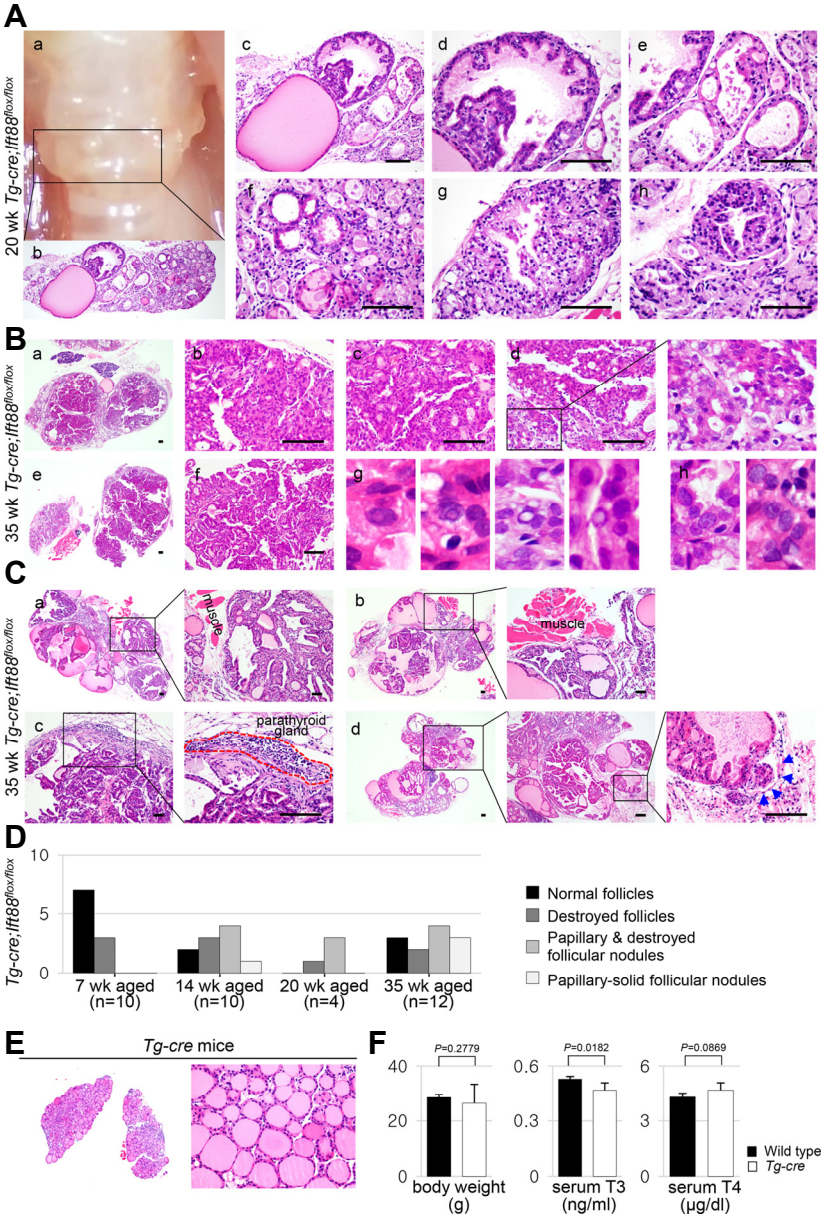

Fig. 6. Papillary-solid proliferative follicular lesions in the murine thyroid with defective *Ift88*-mediated ciliary loss resemble thyroid carcinoma. (A) At 20 weeks of age, the gross morphology of the *Tg-Cre;Ift88*$^{flox/flox}$ thyroid showed a bubble wrap-like appearance (a). Histologically, it showed cystically dilated follicles containing dense colloid (b, c). Dilated follicles with papillary epithelial hyperplasia show scant colloid or clumped Tg globules (d-h). (B) At 35 weeks of age, the *Tg-Cre;Ift88*$^{flox/flox}$ thyroid showed proliferative nodules with papillary-solid growth patterns (a-f). The follicular epithelial cells had nuclear pseudoinclusions (g) and prominent macronucleoli (h). (C) At 35 weeks of age, the proliferative follicular nodules expanded into the perithyroidal skeletal muscle or parathyroid gland (a-c). Vascular invasion of tumor emboli was also observed (d). Scale bar: 100 μm. (D) The phenotypes of the thyroid in *Tg-Cre;Ift88*$^{flox/flox}$ mice were summarized by age group. (E) No significant differences in morphology and function were observed between the *Tg-Cre* transgenic and wild-type control thyroid glands. (F) Body weight was 28.5 ± 1.0 g in wild-type mice and 26.37 ± 6.89 g in *Tg-Cre* transgenic mice. Serum T3 concentration was 0.53 ± 0.02 ng/ml in wild-type mice and 0.47 ± 0.04 ng/ml in *Tg-Cre* transgenic mice. Serum T4 concentration was 4.29 ± 0.19 μg/dl in wild-type mice and 4.66 ± 0.41 μg/dl in *Tg-Cre* transgenic mice.

or solid growing follicles, was zero (0/10) in 7-week-old mice, 50% (5/10) in 14-week-old mice, 75% (3/4) in 20-week-old mice, and 58% (7/12) in 30-week-old mice.

To determine whether atypical follicular changes are induced by the adverse effect of Cre-recombinase, we analyzed *Tg-Cre* transgenic mice. No significant differences in morphology or function were observed between *Tg-Cre* transgenic and wild-type control thyroids (Figs. 6E and 6F).

DISCUSSION

The present study analyzed the distribution of primary cilia in the normal and cancerous thyroid gland in humans and mice. We showed that primary cilia play a critical role in maintaining the structural integrity of thyroid follicles, and that loss of primary cilia contributes to malignant transformation in the murine thyroid gland.

Primary cilia are required for organ development (Fry et al., 2014; Gerdes et al., 2009; Guo et al., 2007). Cardiac primary cilia are necessary for mechanosensing, flow integration, cardiac morphogenesis, and cardiac function (Koefoed et al., 2014; Slough et al., 2008). Lack of murine cardiac primary cilia results in embryonic lethality due to intracardiac defects (Slough et al., 2008). Deficiency of primary cilia in the developing brain is manifested by defects in brain patterning and cerebellar granule neuron precursor proliferation (Guemez-Gamboa et al., 2014; Han and Alvarez-Buylla, 2010). However, the present murine thyroid model of defective *Ift88*-mediated ciliary loss showed no abnormalities in development or folliculogenesis.

Thyroid follicular cells have a structural polarity characterized by the localization of the NIS to the basal surface and pendrin to the luminal surface, and this polarity is essential to maintain proper hormonogenesis. Thyroid-specific *Ift88*-deficient mice showed an irregularly dilated thyroid gland with destroyed follicles, which exhibited empty colloid and reduced *Nis* and *Pendrin* expression. We previously showed that the polarity protein CDC42 is significantly decreased in thyroid cancer cell lines with ciliary loss (Lee et al., 2018). Taken together, these findings indicate that the primary cilia of thyroid follicular cells play a role in maintaining the globular shape of follicles by acting on cell polarity. These findings are consistent with results suggesting that primary cilia determine the planar cell polarity of the inner ear (Jones and Chen, 2008).

We demonstrated that loss of primary cilia is associated with tumorigenesis in the thyroid gland. Previous studies showed that LOF of primary cilia is associated with tumor progression or aggressiveness (Bailey et al., 2009; Degnim et al., 2015). However, these studies did not demonstrate that LOF of primary cilia directly leads to tumor development. These studies suggested that ciliary loss alone is insufficient for tumorigenesis, whereas it may have an effect when accompanied by other signaling abnormalities (Wong et al., 2009). Unlike previous studies, in the present study, we showed that thyroid-specific *Ift88*-deficient mice develop thyroid cancer without additional activation of thyroid oncogenic kinases.

Thyroid cancers originating from follicular epithelial cells can be classified based on histopathological findings such as DTC (including PTC and FTC), PDTC, and ATC. DTCs have a relatively good prognosis, whereas PDTC and ATC are among the most aggressive cancers, which have a median survival rate of less than 6 months. The primary cilium is well preserved in DTC, whereas it is markedly reduced in PDTC or ATC. Consistently, the present ssGSEA of human thyroid cancers showed a significant decrease in primary cilia-specific genes in ATC compared with those in DTC. These results indicate that LOF of *Ift88*/primary cilia may play an important role in the progression from DTC to PDTC or ATC. In thyroid follicular cell-specific *Ift88*-deficient mice, the irregularly dilated and destroyed follicles rapidly progressed, resulting in the formation of papillary-solid hyperplastic follicular nodules. Proliferative follicular cells were characterized by architectural disarray, cellular pleomorphism, atypical nuclei, and vascular invasion, which are pathological features suggestive of malignant transformation. LOF of *Ift88*/primary cilia in murine thyroid follicular cells caused thyroid carcinogenesis with morphological and molecular features similar to those of PDTC or ATC. Therefore, *Tg-Cre;Ift88*$^{flox/flox}$ mice are valuable as a mouse model of unique thyroid cancer.

High TSH causes thyroid hyperplasia/hypertrophy, which can promote the genesis of neoplasia and carcinogenesis of the thyroid. Contrary to other murine thyroid cancer models showing highly upregulated TSH levels, thyroid cancer arising from defective *Ift88*-mediated ciliary loss did not show significant alterations in serum T3 and TSH levels. This suggests that the thyroid carcinogenesis caused by defective *Ift88*-mediated ciliary loss was independent from TSH stimulation.

Because IFT88 functions as a tumor suppressor (Bonura et al., 1999; Wong et al., 2009), LOF of IFT88 affects ciliogenesis as well as tumor suppression. The murine pancreas and kidney with defective *Ift88*-mediated ciliary loss show dilated ducts but no cancer development (Cano et al., 2004; Yoder, 2007). Tumor development associated with defective *Ift88*-mediated ciliary loss may be regarded as an organ-specific process.

In conclusion, LOF of primary cilia in thyroid follicular cells prevented the maintenance of normal follicle structure, resulting in irregularly dilated and destroyed follicles. In these structurally abnormal follicles, the function of thyroid-specific genes was lost and malignant transformation was induced. Papillary-solid proliferative thyroid nodules progressed to aggressive and dedifferentiated thyroid carcinomas.

Note: Supplementary information is available on the Molecules and Cells website (www.molcells.org).

ACKNOWLEDGMENTS

JL was supported by a grant from the Basic Science Research Program through the National Research Foundation of Korea (NRF) funded by the Ministry of Science, ICT (MISIT) (grant number: NRF-2015R1C1A1A02037434), and a grant from the Daejeon St. Mary's Hospital (2018). MS was supported by a grant from the NRF funded by the Ministry of Science and ICT (grant number: NRF-2014M3A9D8034464) and a grant from NRF/MISIT of Korea (grant number: NRF-

2015M3A9B3028218).

REFERENCES

Bailey, J.M., Mohr, A.M., and Hollingsworth, M.A. (2009). Sonic hedgehog paracrine signaling regulates metastasis and lymphangiogenesis in pancreatic cancer. Oncogene *28*, 3513-3525.

Bonura, C., Paterlini-Brechot, P., and Brechot, C. (1999). Structure and expression of Tg737, a putative tumor suppressor gene, in human hepatocellular carcinomas. Hepatology *30*, 677-681.

Cano, D.A., Murcia, N.S., Pazour, G.J., and Hebrok, M. (2004). Orpk mouse model of polycystic kidney disease reveals essential role of primary cilia in pancreatic tissue organization. Development *131*, 3457-3467.

Christensen, S.T., Pedersen, L.B., Schneider, L., and Satir, P. (2007). Sensory cilia and integration of signal transduction in human health and disease. Traffic *8*, 97-109.

Degnim, A.C., Nassar, A., Stallings-Mann, M., Keith Anderson, S., Oberg, A.L., Vierkant, R.A., Frank, R.D., Wang, C., Winham, S.J., Frost, M.H., et al. (2015). Gene signature model for breast cancer risk prediction for women with sclerosing adenosis. Breast Cancer Res. Treat. *152*, 687-694.

Egeberg, D.L., Lethan, M., Manguso, R., Schneider, L., Awan, A., Jorgensen, T.S., Byskov, A.G., Pedersen, L.B., and Christensen, S.T. (2012). Primary cilia and aberrant cell signaling in epithelial ovarian cancer. Cilia *1*, 15.

Ferkol, T.W., and Leigh, M.W. (2012). Ciliopathies: the central role of cilia in a spectrum of pediatric disorders. J. Pediatr. *160*, 366-371.

Fry, A.M., Leaper, M.J., and Bayliss, R. (2014). The primary cilium: guardian of organ development and homeostasis. Organogenesis *10*, 62-68.

Gerdes, J.M., Davis, E.E., and Katsanis, N. (2009). The vertebrate primary cilium in development, homeostasis, and disease. Cell *137*, 32-45.

Guemez-Gamboa, A., Coufal, N.G., and Gleeson, J.G. (2014). Primary cilia in the developing and mature brain. Neuron *82*, 511-521.

Guo, G., Roettger, M.E., and Shih, J.C. (2007). Contributions of the DAT1 and DRD2 genes to serious and violent delinquency among adolescents and young adults. Hum. Genet. *121*, 125-136.

Han, Y.G., and Alvarez-Buylla, A. (2010). Role of primary cilia in brain development and cancer. Curr. Opin. Neurobiol. *20*, 58-67.

Han, Y.G., Kim, H.J., Dlugosz, A.A., Ellison, D.W., Gilbertson, R.J., and Alvarez-Buylla, A. (2009). Dual and opposing roles of primary cilia in medulloblastoma development. Nat. Med. *15*, 1062-1065.

Hassounah, N.B., Bunch, T.A., and McDermott, K.M. (2012). Molecular pathways: the role of primary cilia in cancer progression and therapeutics with a focus on Hedgehog signaling. Clin. Cancer Res. *18*, 2429-2435.

Hassounah, N.B., Nagle, R., Saboda, K., Roe, D.J., Dalkin, B.L., and McDermott, K.M. (2013). Primary cilia are lost in preinvasive and invasive prostate cancer. PloS one *8*, e68521.

Jones, C., and Chen, P. (2008). Primary cilia in planar cell polarity regulation of the inner ear. Curr. Top. Dev. Biol. *85*, 197-224.

Katoh, Y., Terada, M., Nishijima, Y., Takei, R., Nozaki, S., Hamada, H., and Nakayama, K. (2016). Overall architecture of the intraflagellar transport (IFT)-B complex containing cluap1/IFT38 as an essential component of the IFT-B peripheral subcomplex. J. Biol. Chem. *291*, 10962-10975.

Kim, J., Dabiri, S., and Seeley, E.S. (2011). Primary cilium depletion typifies cutaneous melanoma *in situ* and malignant melanoma. PloS one *6*, e27410.

Kobayashi, T., Nakazono, K., Tokuda, M., Mashima, Y., Dynlacht, B.D., and Itoh, H. (2017). HDAC2 promotes loss of primary cilia in pancreatic ductal adenocarcinoma. EMBO Rep *18*, 334-343.

Koefoed, K., Veland, I.R., Pedersen, L.B., Larsen, L.A., and Christensen, S.T. (2014). Cilia and coordination of signaling networks during heart development. Organogenesis *10*, 108-125.

Lee, J., Yi, S., Kang, Y.E., Chang, J.Y., Kim, J.T., Sul, H.J., Kim, J.O., Kim, J.M., Kim, J., Porcelli, A.M., et al. (2016). Defective ciliogenesis in thyroid hurthle cell tumors is associated with increased autophagy. Oncotarget *7*, 79117-79130.

Lee, J., Yi, S., Won, M., Song, Y.S., Yi, H.S., Park, Y.J., Park, K.C., Kim, J.T., Chang, J.Y., Lee, M.J., et al. (2018). Loss-of-function of IFT88 determines metabolic phenotypes in thyroid cancer. Oncogene. *37*, 4455-4474.

Menzl, I., Lebeau, L., Pandey, R., Hassounah, N.B., Li, F.W., Nagle, R., Weihs, K., and McDermott, K.M. (2014). Loss of primary cilia occurs early in breast cancer development. Cilia *3*, 7.

Radford, R., Slattery, C., Jennings, P., Blacque, O., Pfaller, W., Gmuender, H., Van Delft, J., Ryan, M.P., and McMorrow, T. (2012). Carcinogens induce loss of the primary cilium in human renal proximal tubular epithelial cells independently of effects on the cell cycle. Am. J. Renal Physiol. *302*, F905-916.

Schraml, P., Frew, I.J., Thoma, C.R., Boysen, G., Struckmann, K., Krek, W., and Moch, H. (2009). Sporadic clear cell renal cell carcinoma but not the papillary type is characterized by severely reduced frequency of primary cilia. Mod. Pathol. *22*, 31-36.

Seeley, E.S., Carriere, C., Goetze, T., Longnecker, D.S., and Korc, M. (2009). Pancreatic cancer and precursor pancreatic intraepithelial neoplasia lesions are devoid of primary cilia. Cancer Res. *69*, 422-430.

Slough, J., Cooney, L., and Brueckner, M. (2008). Monocilia in the embryonic mouse heart suggest a direct role for cilia in cardiac morphogenesis. Dev. Dyn. *237*, 2304-2314.

Taschner, M., Weber, K., Mourao, A., Vetter, M., Awasthi, M., Stiegler, M., Bhogaraju, S., and Lorentzen, E. (2016). Intraflagellar transport proteins 172, 80, 57, 54, 38, and 20 form a stable tubulin-binding IFT-B2 complex. EMBO J. *35*, 773-790.

Wong, S.Y., Seol, A.D., So, P.L., Ermilov, A.N., Bichakjian, C.K., Epstein, E.H., Jr., Dlugosz, A.A., and Reiter, J.F. (2009). Primary cilia can both mediate and suppress Hedgehog pathway-dependent tumorigenesis. Nat. Med. *15*, 1055-1061.

Yoder, B.K. (2007). Role of primary cilia in the pathogenesis of polycystic kidney disease. J. Am. Soc. Nephrol. *18*, 1381-1388.

Yoo, S.K., Lee, S., Kim, S.J., Jee, H.G., Kim, B.A., Cho, H., Song, Y.S., Cho, S.W., Won, J.K., Shin, J.Y., et al. (2016). Comprehensive analysis of the transcriptional and mutational landscape of follicular and papillary thyroid cancers. PLoS Genet. *12*, e1006239.